Cancer Research

MetaLnc9 Facilitates Lung Cancer Metastasis via a PGK1-Activated AKT/mTOR Pathway

Tao Yu[1], Yingjun Zhao[2], Zhixiang Hu[2], Jing Li[1], Dandan Chu[1], Jiwei Zhang[2], Zhe Li[2], Bing Chen[2], Xiao Zhang[1], Hongyu Pan[1], Shengli Li[2], Hechun Lin[1], Lei Liu[1], Mingxia Yan[1], Xianghuo He[2], and Ming Yao[1]

Abstract

Long noncoding RNAs (lncRNA) participate in carcinogenesis and tumor progression in lung cancer. Here, we report the identification of a lncRNA signature associated with metastasis of non–small cell lung cancer (NSCLC). In particular, elevated expression of LINC00963 (MetaLnc9) in human NSCLC specimens correlated with poor prognosis, promoted migration and invasion of NSCLC cells *in vitro*, and enhanced lung metastasis formation *in vivo*. Mechanistic investigations showed that MetaLnc9 interacted with the glycolytic kinase PGK1 and prevented its ubiquitination in NSCLC cells, leading to activation of the oncogenic AKT/mTOR signaling pathway. MetaLnc9 also interacted with P54nrb/NonO (NONO) to help mediate the activity of CRTC, a coactivator for the transcription factor CREB, reinforcing a positive feedback loop for metastasis. Taken together, our results establish MetaLnc9 as a driver of metastasis and a candidate therapeutic target for treating advanced NSCLC. *Cancer Res; 77(21); 5782–94. ©2017 AACR.*

Introduction

Lung cancer is the leading cause of cancer-related deaths worldwide, especially in China (1). As the predominant form of lung cancer, non–small cell lung cancer (NSCLC) accounts for approximately 85% of lung cancer cases, whereas the frequency of small-cell lung cancer in many countries has been decreasing over the last two decades (2). Despite various clinical advances in systematic therapies for lung cancer patients, the 5-year survival rate remains low (3). Approximately 90% of patients diagnosed with NSCLC die due to distant metastases rather than primary tumor, and metastasis has been a consistent problem in tumor prognosis and therapy (4, 5). However, the complicated molecular and cellular mechanisms involved in lung cancer metastasis remain poorly understood. The need to identify potential therapeutic targets to improve NSCLC treatment is urgent.

Long noncoding RNAs (lncRNA) are transcripts longer than 200 bp that do not encode proteins (6) and participate in controlling fundamental biological processes by regulating gene expression at almost all levels, including epigenetic (7), transcriptional, and posttranscriptional levels (8). The aberrant expression of lncRNAs has been connected to multiple malignancies, including cancer (9–12), providing new insights into cancer development and progression. For example, lnc-DC plays a critical role in dendritic cell differentiation by binding to STAT3 (13). HBXIP and LSD1, which form a complex scaffolded by HOTAIR, activate c-Myc target genes in breast cancer cells (14). lncRNA CCAT2, which is overexpressed in colorectal cancer, promotes metastasis, growth, and chromosomal instability in colon cancer cells through TCF L2-mediated transcriptional regulation (15). lincRNA-p21 functions as a suppresser gene in the p53-transcription pathway and modulates the Warburg effect by cooperating with HIF-1α (16). LINC00473 is consistently the most highly induced gene in LKB-inactivated human primary NSCLC samples and can be integrated into clinical treatment evaluation (17). Lnc-Hc binds hnRNPA2B1 to regulate Cyp7a1 and Abca1 expression in hepatocyte cholesterol metabolism (18). However, the potential regulation and functions of lncRNAs in NSCLC progression remain largely unknown.

In our study, a highly metastatic cell line, SPC-A-1sci, was derived from SPC-A-1 cells (a weakly metastatic cell line) through *in vivo* selection in a NOD/SCID mouse model (19). For the parallel genetic background between these two cell lines, they were used to perform global lncRNAs profiling with microarray analysis to screen metastasis-associated lncRNAs that might be potential therapeutic targets for NSCLC. MetaLnc9 was identified to be significantly upregulated in highly metastatic cells (SPC-A-1sci) and NSCLC tumor tissues, and its expression correlated with distant metastasis and tumor node metastasis. The biological role of MetaLnc9 in lung cancer cells was assessed genetically both *in vitro* and *in vivo*. MetaLnc9 directly interacted with phosphoglycerate kinase 1 (PGK1) and inhibited its ubiquitin-mediated degradation, leading to the activation of the AKT/mTOR signaling pathway in NSCLC cells. Moreover, MetaLnc9 participated in the NONO/CRTC/CREB1 complex and transcriptionally regulated its own expression in NSCLC cells. Our expression, functional, and mechanistic data demonstrate that MetaLnc9 is a potentially

[1]State Key Laboratory of Oncogenes and Related Genes, Shanghai Cancer Institute, Renji Hospital, Shanghai Jiao Tong University School of Medicine, Shanghai, China. [2]Fudan University Shanghai Cancer Center and Institutes of Biomedical Sciences, Shanghai Medical College, Fudan University, Shanghai, China.

Note: Supplementary data for this article are available at Cancer Research Online (http://cancerres.aacrjournals.org/).

T. Yu and Y. Zhao contributed equally to the article.

Corresponding Authors: Ming Yao, Shanghai Cancer Institute, Renji Hospital, Shanghai Jiao Tong University School of Medicine, No. 25/2200, Xietu Road, Shanghai 200032, China. Phone: 86-21-6418-3618; Fax: 86-21-6404-2002; E-mail: myao@shsci.org; and Xianghuo He, Fudan University Shanghai Cancer Center and Institutes of Biomedical Sciences, Shanghai Medical College, Fudan University, xhhe@fudan.edu.cn.

doi: 10.1158/0008-5472.CAN-17-0671

robust biomarker for NSCLC metastasis and a novel gene regulator in NSCLC cells.

Materials and Methods

Cell lines and cell culture

The human NSCLC cell lines H1299, H292, and human embryonic kidney 293T cells used in this study were obtained from the ATCC in 2010. SPC-A-1 was obtained from Cellular Institute of Chinese Academy of Science (Shanghai, China) in 2007. SPC-A-1sci was, a highly metastatic cell line established by our laboratory, was derived from SPC-A-1 cells (a weakly metastatic cell line) through *in vivo* selection in a NOD/SCID mouse model in 2009. All of them were routinely cultured at 37°C in a humidified air atmosphere containing 5% carbon dioxide in DMEM supplemented with 10% FBS (Biowest), 100 μ/mL penicillin (Sigma-Aldrich), and 100 μg/mL streptomycin (Sigma-Aldrich). All the cell lines were used within 20 passages and thawed fresh every 2 months. These cell lines were *Mycoplasma*-free and authenticated by quality examinations of morphology and growth profile.

Human NSCLC samples

The 73-paired human NSCLC and their matched adjacent noncancerous tissues used to analyze MetaLnc9 RNA levels were collected from the Department of Lung Cancer, Shanghai Chest Hospital affiliated to Shanghai Jiao-tong University. The matched adjacent noncancerous were taken at a distance of at least 3 cm from the tumor. Upon resection, Human surgical specimens were immediately frozen in liquid nitrogen and stored at −80°C refrigerator for further investigation. All human specimens were approved by the Ethical Review Committee of the World Health Organization of the Collaborating Center for Research in Human Production authorized by the Shanghai Municipal Government and obtained with informed consent from all patients. This study was approved by the Ethics Committee of Shanghai Jiao-tong University.

5′ and 3′ rapid amplification of cDNA ends analysis

5′- and 3′-rapid amplification of cDNA ends (RACE) analyses were performed with 1 μg of total RNA or poly A+ RNA using the SMARTer RACE 5′/3′ Kit (Clonetech) according to the manufacturer's instructions. The gene-specific primers and nested gene-specific primers used for nested PCR are presented in Supplementary Table S1 They were designed according to the manual guidelines.

RNA extraction and qRT-PCR analysis

Total RNA samples from the NSCLC tissue specimens and cell lines in this study were extracted with TRIzol reagent (Invitrogen, CA) according to the manufacturer's protocol, and quantified with Nanodrop 2000 (Thermo). First-strand cDNA was synthesized with the PrimeScript RT Reagent Kit (TaKaRa). Real-time polymerase chain reaction (qPCR) was performed with SYBR Green Premix Ex Taq (TaKaRa). Relative RNA expression levels determined by qPCR were measured by ABI Prism 7900 sequence detection system (Applied Biosystems). The sequences for the gene-specific primers used are listed in Supplementary Table S1. β-Actin was used as the internal control.

Northern blot

A total of 10 μg of the total RNA was subjected to formaldehyde gel electrophoresis and transferred to a Hybond-N+ membrane (GE Healthcare) by capillary transfer. Membrane was ultraviolet-crosslinked. Digoxin-labeled RNA probes were prepared with the DIG Northern Starter Kit (Roche). The sequences for the primers are listed in Supplementary Table S1. After 60 minutes of pre-hybridization in ULTRAhyb-Oligo buffer (Ambion) at 62°C, the membrane was hybridized for 12 hours at 68°C in ULTRAhyb-Oligo buffer containing the denatured probe. After washing, signal on the membrane was detected using phosphorimaging (Typhoon, Molecular Devices).

Subcellular fractionation

One$\sim 10^7$ cells were collected using 2.5% trypsin and washed once in PBS. According to the PARISTM Kit (Ambion), the cell pellets were incubated with 500 μL Cell Fractionation Buffer on ice 10 minutes, then loosened by flicking the tube. The samples were centrifuged 5 minutes at 4°C with a low speed to keep the nuclei intact. Put the supernatant in a fresh RNase-free tube to isolate cytoplasmic RNA. After removing the supernatant, the Cell Fractionation Buffer was added into the tube to wash the nuclear pellet once. At last, the nuclear pellet was lysed by the ice-cold Cell Disruption Buffer. Cytoplasmic and nuclear fractions were split for RNA extraction and qPCR. The sequences for the primers are listed in Supplementary Table S1.

RNA interference

The siRNA oligonucleotides targeting MetaLnc9, PGK1, NONO (Supplementary Table S1) were designed and synthesized by RiboBio. Cells were transfected with the indicated siRNAs using Lipofectamine 2000 Reagents (Invitrogen), according to the manufacturer's protocol. After transfection for 48 hours, the cells were used for migration, invasion, RNA extraction, and immunoblotting assays,

Vector construction

Full-length MetaLnc9 cDNA was commercially synthesized (GENEWIZ), then was cloned and inserted into the lentiviral expression vector pWPXL. To produce lentivirus containing MetaLnc9, 293T cells were cotransfected with the pWPXL-MetaLnc9 and the lentiviral vector packaging system using Lipofectamine 2000. PGK1 CDS and NONO CDS were amplified using primers depicted in Supplementary Table S1. PGK1 and NONO were, respectively, inserted into pCMV-Flag vector or pCDH-CMV-puro vector, short for pCDH. The sequence of the full-length MetaLnc9 promoter was amplified from −2000 bp to +310 bp; the deletion plasmids were amplified from −2000 bp, −1130 bp, −178 bp, and −30 bp to +310 bp. The mutant was generated by mutating the DNA-binding site (−245 bp to −252 bp). These promoter sequences were all cloned into the pGL3-basic at the *MIu*I and *Xho*I sites.

Cell migration and invasion assays

Cell migration and invasion assays were detected in a 24-well plate with 8-μm-pore size chamber inserts (Corning). For migration assays, 5×10^4 cells were suspended into the upper chamber per well with the non-coated membrane. For invasion assays, 1×10^5 cells were placed into the upper chamber per well with the Matrigel-coated membrane, which was diluted with serum-free culture medium. In both assays, Cells were suspended in 200 μL of DMEM without FBS. In the lower chamber, 800 μL of DMEM supplemented with 10% FBS was added. After 18 hours of incubation at 37°C, the cells, which had migrated to the bottom

surface of the membrane, were fixed with 100% methanol, and stained with 0.1% crystal violet for 20 minutes. Then, the cells were imaged and counted under a CKX41 inverted microscope (Olympus, Japan).

Xenograft model

Five-week-old BALB/c-nu/nu nude male mice were used for animal studies, and all animals were maintained in the pathogen-free (SPF) conditions at shanghai cancer institution. The GFP-Luc lentiviral vector encoding a fusion gene of GFP and luciferase was generated by inserting the GFP-Luc gene from the plasmid eGFP-2A-CBGr99 (kindly provided by Professor Hammerling) into the *Bam*HI/*Xho*I sites of a pWPXL vector. To collect the real-time data of in vivo assays, some special SPC-A-1 cells were transfected with the GFP-Luc lentiviral vector, nominated as SPC-A-1-GFP-Luc cells. The SPC-A-1-GFP-Luc cells were introduced with lentivirus carrying MetaLnc9 or the empty control, then injected into the lateral tail veins of nude mice (12/group). After 6 weeks, all living mice were subjected to analyze the luciferase signal, with subcutaneous injection of the luciferase substrate into the abdomen. When these mice were sacrificed, the resected lung tissues were continuously analyzed for the GFP signal. Then the lung tissues were fixed in 10% neutral PB-buffered formalin. The fixed samples were embedded in paraffin and stained with hematoxylin and eosin. All animal experiments were housed and performed according to the guidelines approved by the Shanghai Medical Experimental Animal Care Commission.

RNA pulldown and mass spectrometry analysis

Biotin-labeled MetaLnc9 was synthesized using the Biotin RNA Labeling Mix by T7 RNA polymerase, and then incubated with the cell lysates for 4 hours. The protein with biotin-labeled MetaLnc9 were pulled down with streptavidin magnetic beads (Thermo) after incubation overnight. The samples were separated using electrophoresis and the specific bands were identified using mass spectrometry and retrieved in human proteomic library. The sequences for the primers are listed in Supplementary Table S1.

RNA Immunoprecipitation

RNA Immunoprecipitation (RIP) experiments were performed using the Magna RIP RNA-Binding Protein Immunoprecipitation Kit (Millipore), according to the manufacturer's instructions. Total RNA (input control) and precipitation with the isotype control (IgG) for each antibody were assayed simultaneously. Five μg antibody against PGK1 and NONO were incubated with the supernatants. The coprecipitated RNAs were pulled down by the protein G beads and then detected by q-PCR. The sequences for the primers are listed in Supplementary Table S1.

Immunoblotting assays

The cell lysates were extracted from cultured cells with RIPA lysis buffer containing protease inhibitors (Byotime). Lysates were cleared by centrifugation at 4°C for 15 minutes at 12,000 × *g*. Protein samples were separated by 6% and 8% sodium dodecyl sulfate (SDS)-PAGE and transferred to nitrocellulose filter membranes (Millipore). After blocking in PBS/Tween-20 containing 5% nonfat milk, the membranes were incubated with the primary antibodies (Supplementary Table S1). Subsequent visualization was detected with SuperSignal West Femto Maximum Sensitivity Substrate (Thermo). The antibodies for the assays are listed in Supplementary Table S2.

Luciferase assays

HEK-293T cells were seeded in 96-well plates at a density of 5,000 cells per well 24 hours before transfection. The cells were co-transfected with a mixture of 50 ng PGL3-basic-MetaLnc9 promoter, 10 ng *Renilla* and 50 ng pCDH-CREB1 or control according to the recommended instruction by using the Lipofectamine 2000. After 48 hours of transfection, Firefly and *Renilla* luciferase activity was measured by the Dual-Luciferase Reporter Assay System (Promega). The relative firefly luciferase activities were detected, and *Renilla* luciferase activities served as an internal control.

Chromatin immunoprecipitation

The cells overexpressing pCDH-Flag-CREB1 were cross-linked by 1% formaldehyde for 10 minutes, cracked with SDS lysis buffer followed by ultransonication with 50 minutes, then incubated with anti-Flag at 4°C overnight. After decrosslinking of the protein–DNA complex, PCR was used to detect the precipitated CREB1-binding sites with specific primers (Supplementary Table S1).

Microarray and expression data analysis

We performed global lncRNAs profiling with microarray analysis to screen metastasis-associated lncRNAs. Data are available via Gene Expression Omnibus (GEO) GSE101836. Online-available datasets were downloaded from NCBI. The expression of MetaLnc9 in 464 NSCLC tissues originated from The Genomic Data Commons Data Portal (https://gdc-portal.nci.nih.gov/). One hundred and seventeen lung adenocarcinoma patients were involved in the Tomida' Cohort (https://www.ncbi.nlm.nih.gov/geo/query/acc.cgi?acc=GSE13213), for NONO expression analysis. The ChIP-seq data for CREB1 were downloaded from ENCODE (https://www.encodeproject.org/).

URLs

The coding potential of the MetaLnc9 transcript was analyzed using PhyloCSF codon substitution frequency analysis (UCSC), the Coding Potential Assessment Tool (CPAT, http://lilab.research.bcm.edu/cpat/index.php) and the coding potential calculator (CPC, http://cpc.cbi.pku.edu.cn/). The MetaLnc9 promoter were analyzed in the JASPAR database (http://jaspar.genereg.net/).

Statistical analysis

Unless stated otherwise, the data are presented as the mean ± SEM from one representative experiment out of three independent experiments, and every representative experiment has three repetitions. Student *t* test or one-way ANOVA was performed to evaluate differences between two groups or between more than two groups, respectively. The Wilcoxon tests were used to analyze MetaLnc9 RNA levels between human NSCLC samples and the matched non-tumorous lung tissues, and the Mann–Whitney tests or Kruskal–Wallis tests were used to analyze MetaLnc9 RNA levels in grouped human samples. ROC curve analysis was used to determine the efficacy of MetaLnc9 in The Cancer Genome Atlas (TCGA) cohort or NONO expression in the Tomida' Cohort, then the log-rank Mantel-Cox test was performed to analyze the correlation between the

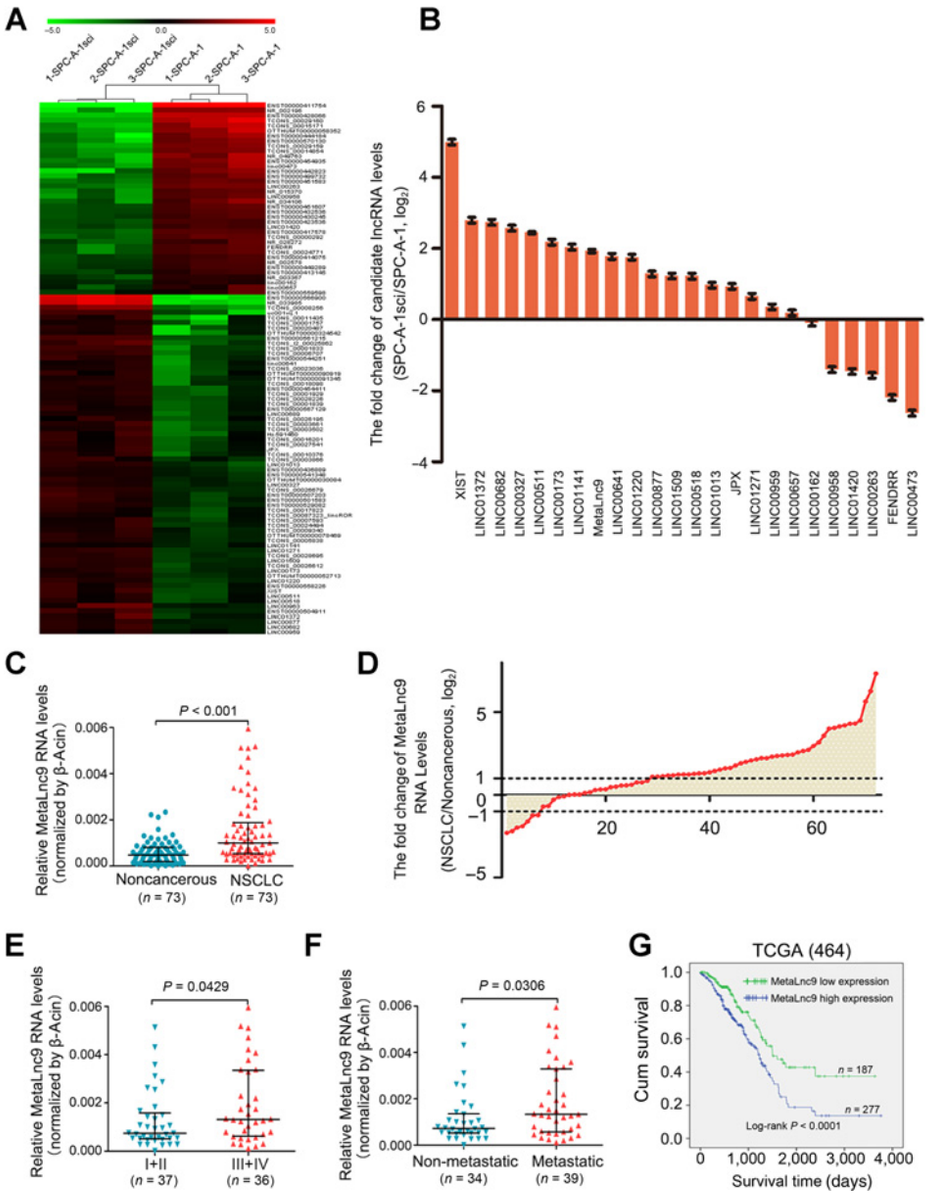

Figure 1.
MetaLnc9 is associated with advanced tumor metastasis in NSCLC. **A,** Heat map representation of RNA-sequencing for gene expression profiles of highly metastatic cells (SPC-A-1sci) and low-metastatic cells (SPC-A-1); For each group, triple biological repeats were analyzed. The detailed annotation as listed in Supplementary Table S3. **B,** Expression levels of candidate lncRNAs in highly metastatic cells (SPC-A-1sci) and low-metastatic cells (SPC-A-1). **C,** MetaLnc9 RNA levels were quantified in 73 pairs of NSCLC tissues and adjacent normal tissues using qPCR. **D,** Fold changes in MetaLnc9 expression in 73 paired tissues (NSCLC/noncancerous; up-expression, >1; no change, -1∼1; down-expression, ←1.). **E** and **F,** Clinical significance of MetaLnc9 in patients with NSCLC; high MetaLnc9 expression was positively correlated with TNM stage (III+IV; **E**) and metastasis (lymph node metastasis and/or distal metastasis; **F**). **G,** Kaplan–Meier analyses of the correlation between MetaLnc9 RNA levels and overall survival in the 464-patient-TCGA cohort. Values represent medians with interquartile range in (**C**, **E**, and **F**). The patients were staged in accordance with the 7th Edition of the AJCC cancer tumor node metastasis classification in **E**. β-Actin served as the control in **B–F**. Values are expressed as mean ± SEM, $n = 3$ in **B–F**.

expression levels and overall survival. Qualitative variables were compared using χ^2 tests. $P < 0.05$ was considered statistically significant. Figures were generated with GraphPad Prism 5 software. All analyses were performed with SPSS software (version 19.0, Armonk).

Results

MetaLnc9 is overexpressed and associated with poor outcomes in NSCLC patients

The highly metastatic SPC-A-1sci cell line in our study was derived from SPC-A-1 using an *in vivo* metastatic selection model (Supplementary Fig. S1A), and the two cell lines share the same genetic background. Using lncRNA microarray assays, we screened both cell lines for metastasis-associated lncRNAs in NSCLC (Fig. 1A; Supplementary Table S3). After verification by quantitative real-time PCR (qRT-PCR) and functional screening (Fig. 1B; Supplementary Table S4), MetaLnc9 was selected as a potential metastasis-related long intergenic noncoding RNA (lincRNA) for NSCLC. MetaLnc9 locates in chromosomal locus 9q34 (20), and has one transcript containing five exons (NR_038955, 2123 nt). However, our 5′ and 3′ RACE assays and quantitative real-time PCR revealed that the 1901-nt transcript is the predominant transcript in NSCLC cell lines and NSCLC tissues, with a shorter 5′ end compared with the annotated transcript (Supplementary Fig. S1B–S1E). Furthermore, the RNA level of this 1901-nt transcript was demonstrably higher in SPC-A-1sci cells than in SPC-A-1 cells according to northern blotting (Supplementary Fig. S1F). The coding potential of the 1901-nt MetaLnc9 transcript was analyzed using PhyloCSF

codon substitution frequency analysis, the Coding Potential Assessment Tool and the coding potential calculator (Supplementary Fig. S2A–S2C). The data strongly suggested that MetaLnc9 is a noncoding RNA. MetaLnc9 was expressed to varying degrees in NSCLC cell lines (Supplementary Fig. S1E), being present in both the cytoplasm and nucleus of SPC-A-1sci cells (Supplementary Fig. S2D).

To assess the clinical significance of MetaLnc9, we analyzed MetaLnc9 RNA levels in 73 pairs of human NSCLC and their corresponding noncancerous lung tissues. Compared with corresponding nontumorous tissues, MetaLnc9 was significantly upregulated in NSCLC tissues (Fig. 1C). Moreover, the RNA expression of MetaLnc9 was upregulated in 61.6% (45/73) of NSCLC cases (Fig. 1D), and its expression was positively correlated with advanced TNM stages (III and IV) and lymph node and distal metastasis (Fig. 1E and F; Supplementary Table S5). The correlation between MetaLnc9 RNA levels and NSCLC clinicopathological features was confirmed in another 464-TCGA-patient cohort (https://cancergenome.nih.gov/, Fig. 1G). Importantly, high levels of MetaLnc9 RNA were remarkably associated with poor outcomes in the 464-TCGA-patient cohort (Fig. 1G). Taken together, our data show that MetaLnc9 is highly expressed in lung cancer and related to clinical severity and prognosis.

MetaLnc9 enhances the migration and invasion abilities of NSCLC cells *in vitro* and *in vivo*

Aside from its identification as a metastasis-related lincRNA from the highly metastatic SPC-A-1sci cell line, the relationship between MetaLnc9 RNA levels and lymph node and distal metastasis also prompted us to explore the effect of this lincRNA on NSCLC cell invasion and metastasis. Stable cell lines (pWPXL-MetaLnc9) were established via lentiviral infection of NSCLC cells (Supplementary Fig. S3A). MetaLnc9 overexpression substantially enhanced the migration and invasion abilities of SPC-A-1 and H292 cells (Fig. 2A and B), but had no impact on SPC-A-1 and H292 cell growth in wells coated with or without Matrigel at the end time point of migration and invasion assays (Supplementary Fig. S3B). Conversely, knocking down endogenous MetaLnc9 in NSCLC cells via two independent siRNAs significantly reduced the migration and invasion abilities of SPC-A-1sci and H1299 cells (Fig. 2C and D; Supplementary Fig. S3C), yet did not change cell proliferation of SPC-A1-sci or H1299 cells under the indicated conditions (Supplementary Fig. S3D). These results indicated that the promotion of migration and invasion by MetaLnc9 was not due to cell proliferation.

To further investigate the effect of MetaLnc9 on NSCLC cell metastasis *in vivo*, SPC-A-1 cells were tagged with the luciferase gene, which can be easily traced by *in vivo* imaging systems. The pWPXL-MetaLnc9 cells and the control cells, both derived from the tagged cells, were injected into the lateral tail veins of nude mice ($n = 12$). After 6 weeks, Bioluminescence Imaging (BLI) showed a significant increase in tumorigenesis and lung metastasis in the pWPXL-MetaLnc9 group (Fig. 2E and F). The mice were then euthanized and their lungs were dissected out for histological analysis; as expected, a higher number of lung metastatic nodules was observed in the pWPXL-MetaLnc9 group compared with the control group (Fig. 2G and H). Taken together, these results demonstrated that MetaLnc9 acts as a driver in the metastasis of NSCLC cells.

MetaLnc9 physically interacts with PGK1 and NONO in NSCLC cells

To elucidate the molecular mechanism underlying how MetaLnc9 promotes metastasis in NSCLC cells, we next identified protein partners of MetaLnc9 in NSCLC cells through RNA pull-down assays. Two independent MetaLnc9 pull-down experiments showed specific bands at approximately 50 and 60 kD (Fig. 3A). These protein bands, which were specifically enriched in MetaLnc9 pull-down assays, were subjected to mass spectrometry, which identified of 7 potential MetaLnc9-interacting proteins based on unique peptides (>2) with repeated appearances (Supplementary Table S6). Immunoblotting independently confirmed that two of the candidates, PGK1 and P54^{nrb}/NonO (NONO), interact directly with MetaLnc9 (Fig. 3B). Moreover, RIP assays also demonstrated that MetaLnc9 was markedly enriched in pull-downs with antibodies against PGK1 and NONO, as determined by measuring coprecipitated RNA by qPCR and RT-PCR with agarose gel electrophoresis analysis (Fig. 3C and D). These results indicated that PGK1 and NONO specifically interact with MetaLnc9 in NSCLC cells.

We next constructed a series of MetaLnc9 deletion mutants based on its secondary structure (Supplementary Fig. S4A) to map the precise binding regions for PGK1 and NONO. According to *in vitro* RNA pull-down assays, the 1∼230 nt fragment in the 5′ arm of MetaLnc9 mediate its association with PGK1 and NONO (Fig. 3E). On the other hand, RIP assays with full-length and truncated PGK1 and NONO showed that the substrate-binding domain of PGK1 and the RRM2 domain of NONO are responsible for their interaction with MetaLnc9 (Fig. 3F and G). However, these two proteins did not bind each other (Supplementary Fig. S4B). Moreover, migration and invasion assays showed that the 1∼230 nt fragment of MetaLnc9 is sufficient for its function in SPC-A-1 and H292 cells (Fig. 3H; Supplementary Fig. S4C), suggesting that the interaction between MetaLnc9 and its partners, PGK1 and NONO, might contribute to the promotion of NSCLC metastasis.

MetaLnc9 had no effect on NONO mRNA and protein levels (Fig. 4A and B). Even though PGK1 mRNA levels were unchanged (Fig. 4A); however, PGK1 protein levels were dramatically reduced when MetaLnc9 was silenced and increased when MetaLnc9 was overexpressed (Fig. 4B; Supplementary Fig. S4D). The protein stability and the half-life of PGK1 protein were dramatically dampened by MetaLnc9 siRNA in SPC-A-1sci and H1299 cells treated with the protein synthesis inhibitor cycloheximide (CHX), and the protein stability of PGK1 were increased when MetaLnc9 was upregulated in SPC-A-1 and H292 cells (Fig. 4C and D; Supplementary Fig. S4E and S4F). Moreover, PGK1 protein degradation in SPC-A-1sci and H1299 cells was accelerated by MetaLnc9 siRNA and suppressed by treatment with the proteasome inhibitor MG132 (Fig. 4E), suggesting that MetaLnc9 inhibits the proteasome-dependent degradation of PGK1 in NSCLC cells. As expected, the ubiquitination of PGK1 in SPC-A-1sci cells was enhanced by MetaLnc9 knockdown but was dramatically reduced in SPC-A-1 cells by MetaLnc9 overexpression (Fig. 4F). These results implicate PGK1 as the downstream target gene of MetaLnc9. When endogenous PGK1 was effectively silenced (Fig. 4G; Supplementary Fig. S4G), the migration and invasion abilities of SPC-A-1sci and H1299 cells were remarkably reduced (Fig. 4H; Supplementary Fig. S4H). Unsurprisingly, PGK1 overexpression rescued the inhibitory effect of MetaLnc9 on NSCLC cell migration and invasion (Fig. 4I). Taken together,

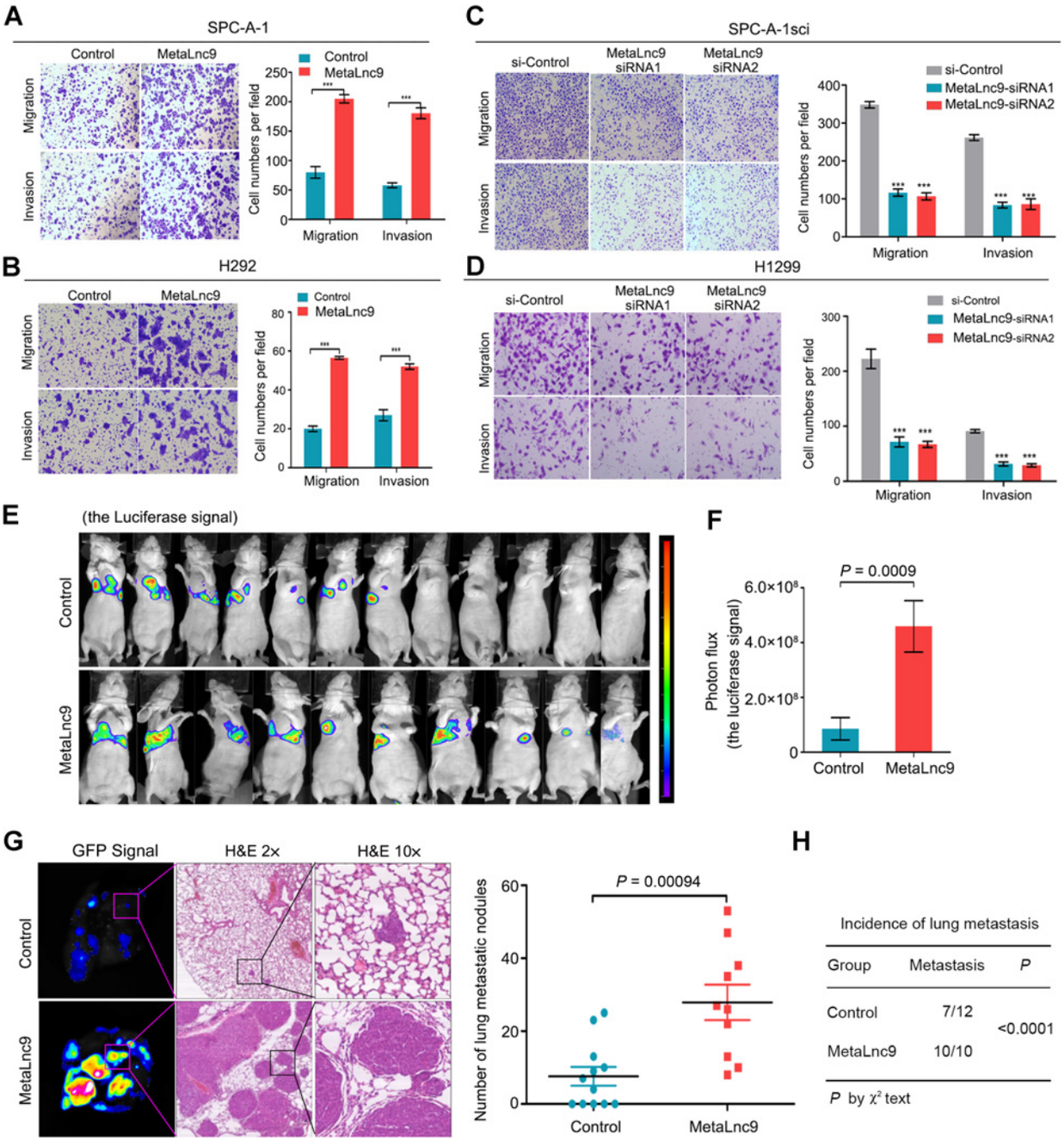

Figure 2.

MetaLnc9 increases NSCLC cell migration, invasion, and metastasis *in vitro* and *in vivo*. **A** and **B,** Transwell migration and invasion assays in stable pWPXL-MetaLnc9 SPC-A-1 and H292 cells. **C** and **D,** Transwell migration and invasion assays in SPC-A-1sci and H1299 cells transfected with two independent MetaLnc9 siRNAs. **E** and **F,** MetaLnc9 overexpression increases lung metastases *in vivo*. Representative bioluminescence images of animals taken before the mice were euthanized. The color scale depicts the photon flux emitted from these mice (**E**); the quantitation of lung metastasis was assessed by bioluminescence measurements (**F**). Two mice died naturally under pathogen-free (SPF) conditions. **G** and **H,** Hematoxylin and eosin (H&E) staining in the lung samples obtained from nude mice after injection with stable pWPXL-MetaLnc9 SPC-A-1 cells (**G**); statistical analysis of lung metastasis in pWPXL-MetaLnc9 and control groups (**H**). Values represent the mean ± SEM, $n = 3$ in **A–D**, $n = 10$–12 in **E–H**; ***, $P < 0.001$.

our results indicate that MetaLnc9 physically interacts with PGK1 and NONO and that PGK1 is the functional downstream target gene of MetaLnc9 in NSCLC cells.

MetaLnc9 regulates the AKT/mTOR signaling pathway via PGK1

To better understanding the molecular mechanisms by which MetaLnc9 enhances the metastatic abilities of NSCLC cells, we

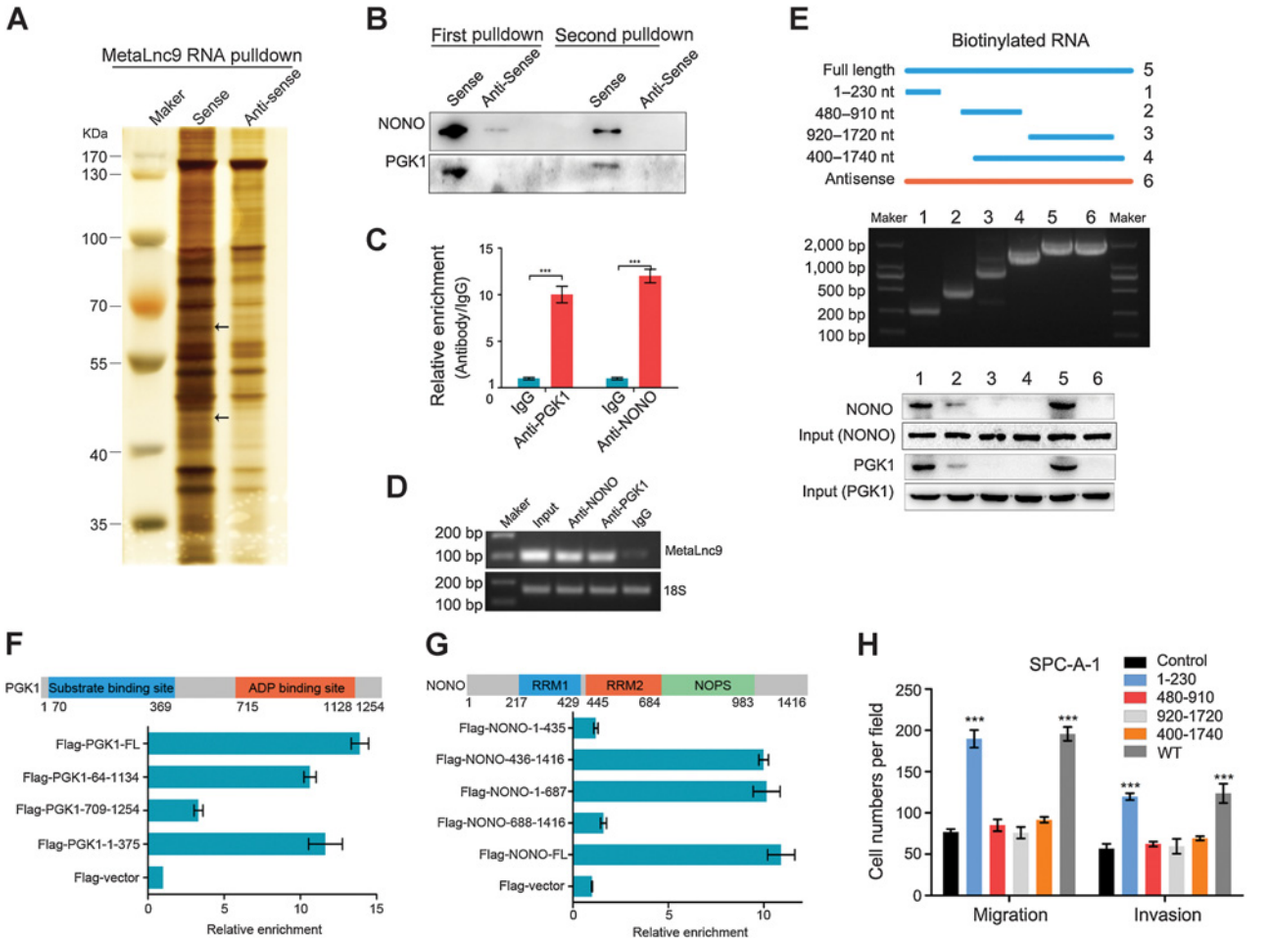

Figure 3.

MetaLnc9 physically interacts with PGK1 and NONO in NSCLC cells. **A,** MetaLnc9-sense and MetaLnc9-antisense probes were biotinylated, transcribed *in vitro*, and incubated with SPC-A-1sci whole-cell lysates for RNA pull-down assays. After silver staining, the 50 and 70-kD MetaLnc9-sense–specific bands (arrows), which repeatedly appeared in two independent assays, were excised and analyzed by mass spectrometry. **B,** Immunoblotting for specific associations of PGK1 or NONO with MetaLnc9 from two independent RNA pull-down assays. **C** and **D,** RIP assays were performed using antibodies against PGK1 or NONO; qPCR (**C**) and RT-PCR (**D**) assays were used to detect MetaLnc9. **E,** Immunoblotting for PGK1 or NONO in samples pulled down with full-length MetaLnc9 (5), truncated MetaLnc9 (1, +1-230 nt; 2, 480-910 nt; 3, 920-1720 nt; 4, 400-1740 nt) or antisense probe (6). **F** and **G,** Deletion mapping to identify the domains of PGK1 (**F**) or NONO (**G**) that bind to MetaLnc9. RIP analysis for MetaLnc9 enrichment in cells transiently transfected with full-length or truncated FLAG-tagged constructs. **H,** Transwell migration and invasion assays in SPC-A-1 cells stably overexpressing full-length or truncated MetaLnc9. Values represent the mean ± SEM, $n = 3$ in **C** and **F–H**; ***, $P < 0.001$.

performed RNA-seq analysis to obtain the transcriptional profiles of SPC-A-1 cells overexpressing MetaLnc9 (Supplementary Table S7). To identify signaling pathways involved in NSCLC metastasis, we performed gene set enrichment analysis (GSEA) to reveal the gene signatures affected by MetaLnc9 (Supplementary Table S8). MetaLnc9 regulated multiple biological process in NSCLC cells (Fig. 5A), especially processes related to cell adhesion. Functional annotations revealed which genes were involved in the cell adhesion process (Fig. 5B), and we confirmed that their mRNA levels were regulated by MetaLnc9 in SPC-A-1 cells (Fig. 5C). The EMT process in SPC-A-1 cells was also confirmed to being markedly affected (Fig. 5D–F) by MetaLnc9 overexpression. Moreover, the PI3K/AKT/mTOR pathway was significantly enriched in GSEA plots, appearing as the top-ranked signaling pathway (Fig. 5G; Supplementary Table S8). Using qPCR, we confirmed alterations in the top-scoring genes following MetaLnc9 overexpression (Fig. 5H and I).

We then examined the effects of MetaLnc9 on AKT/mTOR signaling by immunoblotting. MetaLnc9 knockdown by specific siRNAs inhibited the phosphorylation of mTOR (Ser2481), 70S6K (Thr389), AKT (Ser473), and ERK (Thr202/Tyr204) in SPC-A-1sci and H1299 cells, whereas MetaLnc9 overexpression significantly promoted the phosphorylation of the corresponding sites of mTOR, 70S6K, AKT, and ERK in SPC-A-1 and H292 cells (Fig. 5J), whereas total amount of mTOR, 70S6K, AKT, and ERK protein levels were not significantly altered. As PGK1 is the functional downstream target gene of MetaLnc9, we determined that PGK1 also contributes to the effect of MetaLnc9 on AKT/mTOR signaling in NSCLC cells (Supplementary Fig. S4I). Moreover, PGK1 over-expression rescued the inhibitory effects of

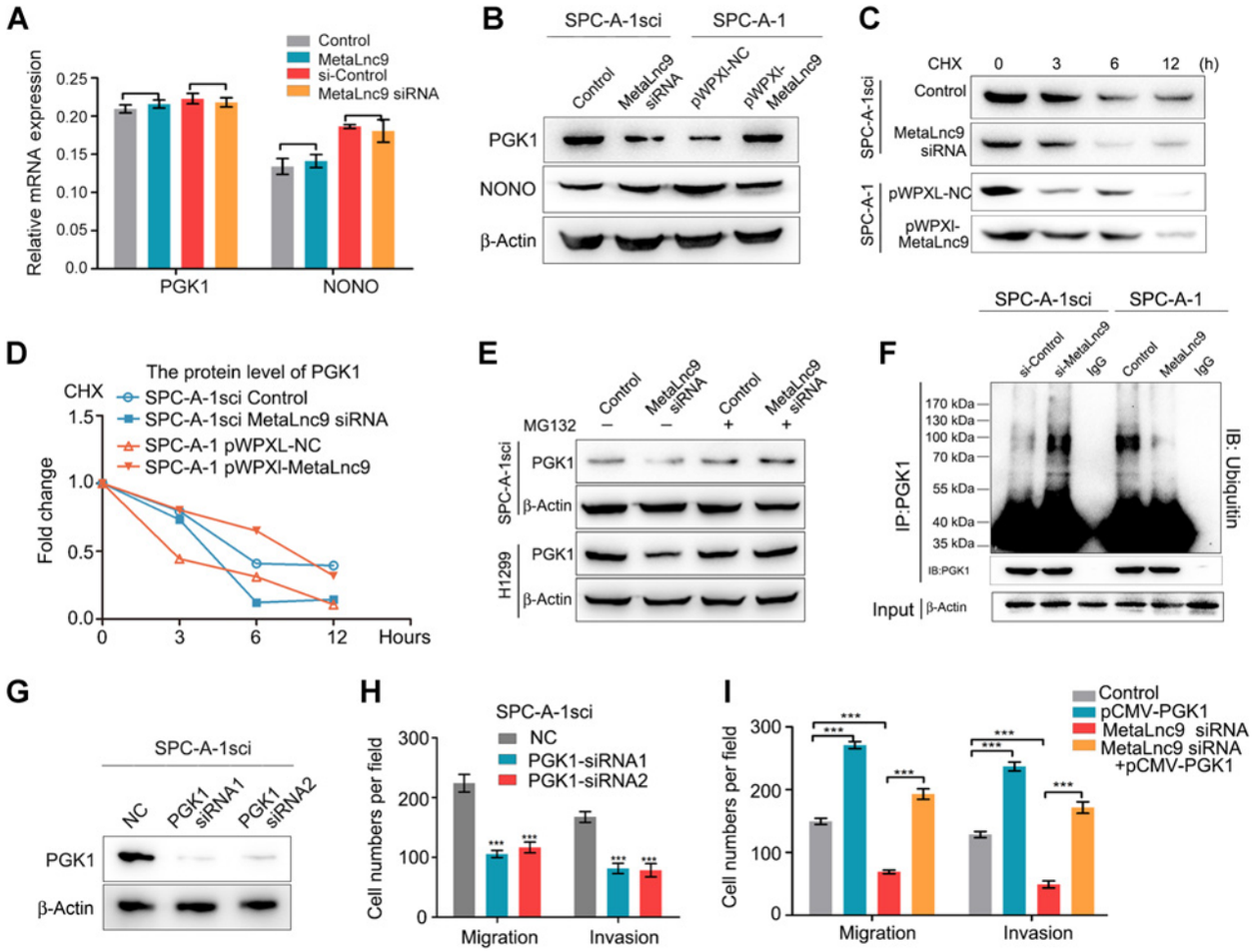

Figure 4.

PGK1 is the functional downstream target of MetaLnc9 in NSCLC cells through physical interaction. **A,** PGK1 and NONO mRNA levels were quantified by qPCR with MetaLnc9 overexpression in SPC-A-1 cells or knockdown in SPC-A-1sci cells. **B,** Immunoblotting for PGK1 and NONO protein levels after MetaLnc9 overexpression in SPC-A-1 cells or knockdown in SPC-A-1sci cells. **C** and **D,** SPC-A-1sci cells transfected with MetaLnc9 siRNA and SPC-A-1 cells transfected with MetaLnc9 overexpression were treated with cycloheximide (CHX, 50 μg/mL) for the indicated times. **C,** Immunoblotting for PGK1 levels in whole-cell extracts. **D,** Densitometry analysis of PGK1 protein levels; the relative fold of the level at 0 hours. **E,** SPC-A-1sci and H1299 cells transfected with MetaLnc9 siRNA were treated with MG132 (25 μmol/L) for 12 hours; immunoblotting for PGK1 levels in the indicated cells. **F,** Cell lysates form SPC-A-1 cells with MetaLnc9 overexpression or SPC-A-1sci cells with MetaLnc9 knockdown were immunoprecipitated (IP) with either control IgG or PGK1 antibody and then immunoblotted for ubiquitin and PGK1. **G,** Immunoblotting for PGK1 protein levels in SPC-A-1sci cells transfected with two independent PGK1 siRNAs. **H,** Transwell migration and invasion assays in SPC-A-1sci cells transfected with PGK1 siRNAs. **I,** Rescue assays for Transwell migration and invasion assays were performed after MetaLnc9 silencing in SPC-A-1 cells transiently expressing PGK1. Values represent the mean ± SEM, $n = 3$ in **A**, **H**, and **I**. β-Actin served as the internal control in **B** and **E–G**; ***, $P < 0.001$.

MetaLnc9 knockdown on AKT/mTOR signaling in SPC-A-1sci cells, whereas the activation of AKT/mTOR signaling by MetaLnc9 overexpression was reversed by PGK1 knockdown in SPC-A-1 cells (Fig. 5K). Collectively, these results demonstrate that MetaLnc9 activates the AKT/mTOR signaling pathway by interacting with PGK1.

NONO regulates MetaLnc9 expression and mediates a feedback loop via CRTC/CREB transcription

Our results demonstrated that NONO interacts with but is not regulated by MetaLnc9. NONO knockdown could inhibit the migration and invasion abilities in SPC-A-1sci and H1299 cells (Supplementary Fig. S5A–S5D) and, consistent with the clinical features of MetaLnc9, patients from Tomida's Cohort with higher NONO expression levels had poorer overall survival (Supplementary Fig. S5E). Therefore, we evaluated whether NONO has some other effect on MetaLnc9. Surprisingly, NONO knockdown dramatically reduced MetaLnc9 RNA levels in SPC-A-1sci and H1299 cells (Fig. 6A) but did not alter MetaLnc9 RNA stability following treatment with the RNA synthesis inhibitor dactinomycin D (Supplementary Fig. S5F), suggesting a role for NONO in the transcriptional regulation of MetaLnc9. According to the chromatin immunoprecipitation sequencing (ChIP-seq) database (21), histone H3K4me3, H3k27ac and RNA polymerase II (Pol II) were enriched near the TSS of MetaLnc9 in A549 cells (Supplementary Fig. S5G), indicating that the MetaLnc9

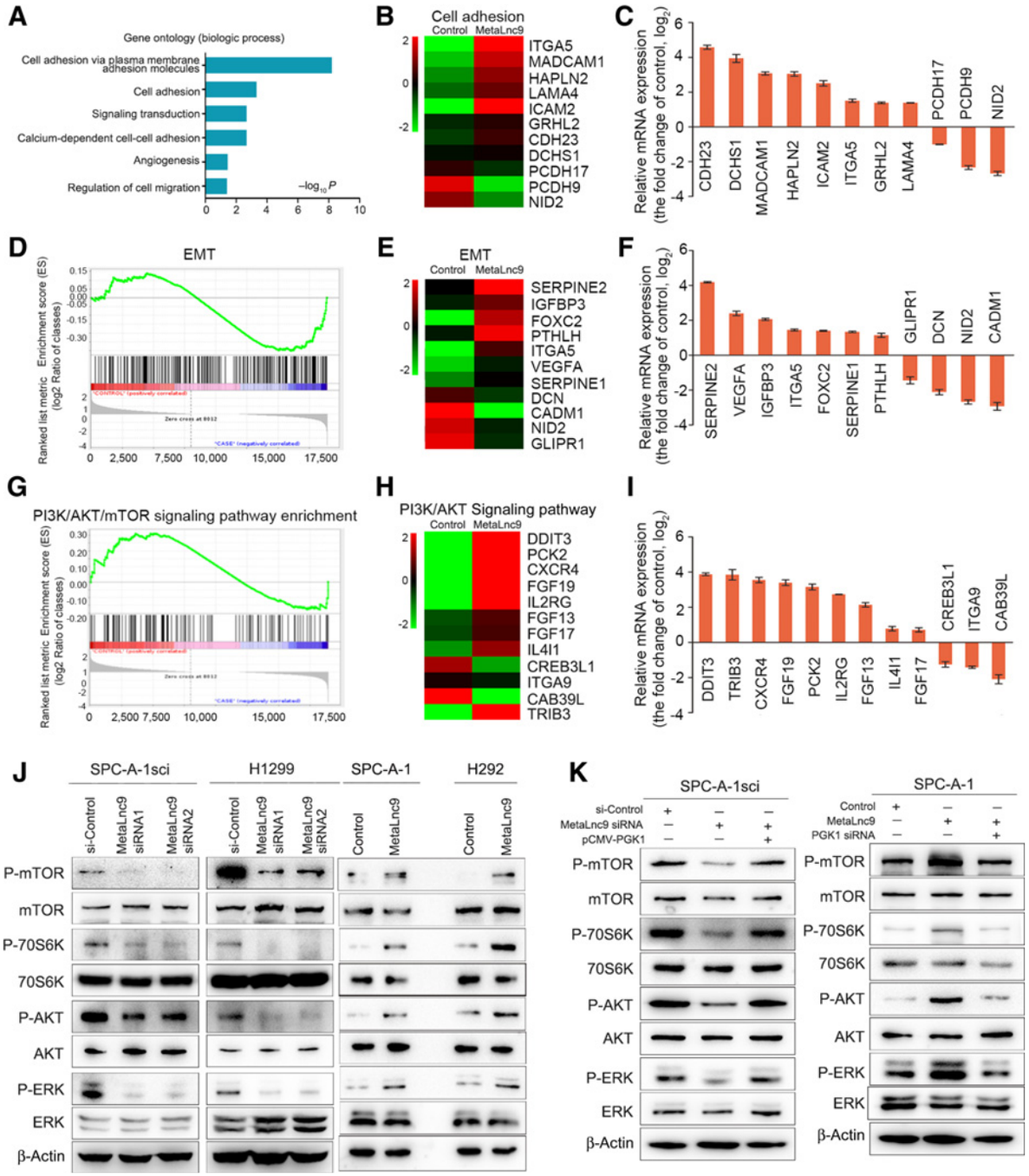

Figure 5.

MetaLnc9 regulates the AKT/mTOR signaling pathway with PGK1 in NSCLC cells. **A,** Functional annotation clustering of genes regulated by MetaLnc9 overexpression in SPC-A-1 cells. Enriched groups listed by their gene ontology term are ranked on the basis of the significant enrichment scores. **B,** Gene expression levels of the subsets of genes for the cell adhesion process from SPC-A-1 cells overexpressing MetaLnc9. Green, black, or red shading in the heat map indicate low, intermediate, or high gene expression, respectively. **C,** qPCR assays for the selected genes from the cell adhesion process in SPC-A-1 cells overexpressing MetaLnc9. **D, E,** and **F,** The EMT process in SPC-A-1 cells overexpressing MetaLnc9; GSEA enrichment (**D**) and gene expression levels (**E**) of the subsets of genes for the process; (**F**) qPCR assays for the selected genes from the process. **G, H,** and **I,** PI3K/AKT/mTOR signaling in SPC-A-1 cells overexpressing MetaLnc9; GSEA enrichment (**G**) and gene-expression levels (**H**) of subsets of genes for the process; qPCR assays for the selected genes from the process (**I**). **J,** Immunoblotting analysis for mTOR (Ser2481), 70S6K (Thr389), AKT (Ser473), and ERK (Thr202/Tyr204) phosphorylation in SPC-A-1sci and H1299 cells transfected with MetaLnc9 siRNAs or in SPC-A-1 and H292 cells stably overexpressing MetaLnc9. **K,** Rescue assays for immunoblotting analysis of mTOR (Ser2481), 70S6K (Thr389), AKT (Ser473), and ERK (Thr202/Tyr204) phosphorylation after MetaLnc9 silencing in SPC-A-1sci cells transiently expressing PGK1 or after PGK1 silencing in SPC-A-1 cells stably overexpressing MetaLnc9. Values represent the mean ± SEM, $n = 3$ in **C**, **F**, and **I**. β-Actin served as the internal control in **J** and **K**.

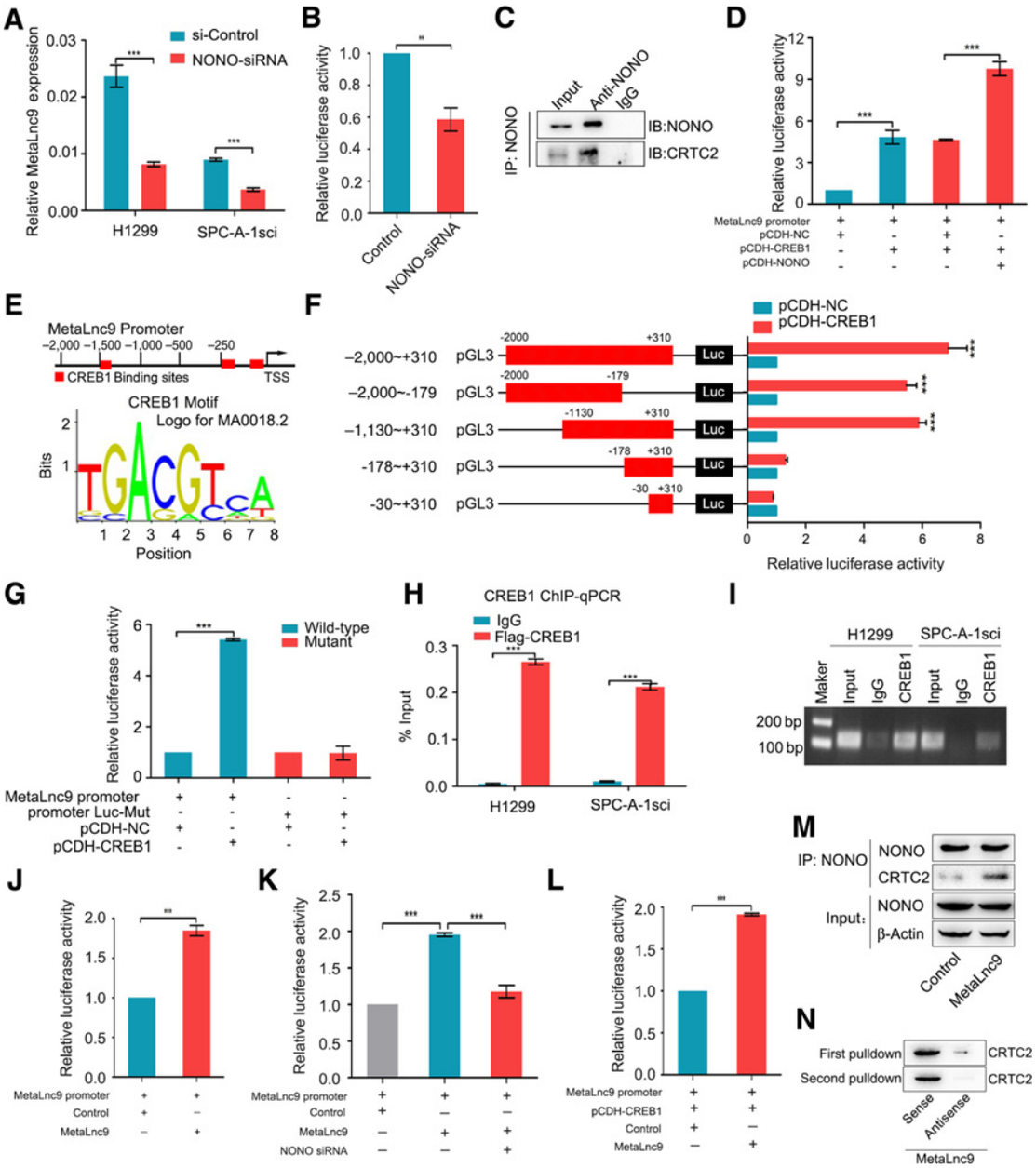

Figure 6.

NONO regulates MetaLnc9 expression through CRTC/CREB transcription and mediates feedback on MetaLnc9 expression. **A,** MetaLnc9 RNA levels were quantified by qPCR in SPC-A-1sci and H1299 cells with NONO siRNAs. **B,** Luciferase activity of the 2.5-kb MetaLnc9 promoter in SPC-A-1sci cells transfected with NONO siRNAs. **C,** Immunoprecipitation assay to identify the association between NONO and CRTC2 in SPC-A-1sci cells. **D,** Luciferase activity of the 2.5-kb MetaLnc9 promoter in SPC-A-1sci cells with stable NONO and/or CREB1 overexpression. **E,** Prediction of potential CREB1-binding sites in the 2.5-kb MetaLnc9 promoter in the JASPAR database (http://jaspar.genereg.net/). Top, a diagram of the 2.5-kb MetaLnc9 promoter with predicted CREB1-binding sites; bottom, the consensus CREB-binding sequence used for the prediction. **F,** Identification of crucial CREB1-binding sites in the MetaLnc9 promoter (left, diagrams of the full-length 2.5-kb MetaLnc9 promoter and the deletion fragments according to the CREB1 motif; right, luciferase activity of the full-length or truncated promoter in SPC-A-1sci cells stably overexpressing CREB1). **G,** Luciferase activity of the 2.5-kb MetaLnc9 promoter, with or without a mutation in the crucial CREB1-binding site, in SPC-A-1sci cells stably overexpressing CREB1. **H** and **I,** ChIP assays for the binding of CREB1 to the crucial CREB1-binding site in the 2.5-kb MetaLnc9 promoter. ChIP products were amplified by qPCR (**H**) and RT-PCR (**I**). **J,** Luciferase activity of the 2.5-kb MetaLnc9 promoter in SPC-A-1 cells with stable MetaLnc9 overexpression. **K,** Luciferase activity of the 2.5-kb MetaLnc9 promoter after overexpressing MetaLnc9 in SPC-A-1 cells with NONO knockdown. **L,** Luciferase activity of the 2.5-kb MetaLnc9 promoter after overexpressing MetaLnc9 in SPC-A-1 cells with stable CREB1 overexpression. **M,** Immunoprecipitation assay to identify the NONO–CRTC2 complex in SPC-A-1 cells with stably overexpressing MetaLnc9. **N,** Immunoblotting for specific binding of CRTC2 to MetaLnc9 in SPC-A-1sci cells. Values represent the mean ± SEM, $n = 3$ in **A**, **B**, **D**, **F**, **G**, **H**, and **J–L**. β-Actin served as the internal control in **M**; **, $P < 0.01$; and ***, $P < 0.001$.

promoter is a typical active promoter. We constructed fragment of the MetaLnc9 promoter (−2000 to +310 nt) into a luciferase reporter vector, and the luciferase activity was obviously suppressed by NONO siRNAs in SPC-A-1sci cells (Fig. 6B). NONO is a nuclear protein that binds to CRTC coactivators, which is essential for CREB-mediated transcription (17, 22), and NONO also been identified to interact with CRTC2 in SPC-A-1sci cells (Fig. 6C). Interestingly, strong CREB1 signals were detected in the MetaLnc9 promoter region in A549 cells (Supplementary Fig. S5G; ENCODE datasets: https://www.encodeproject.org/, GEO: GSM1010726). CREB enhanced the luciferase activity of a 2.5-kb region of the MetaLnc9 promoter in SPC-A-1sci cells, which was further enhanced by cotransfection with CREB1 and NONO (Fig. 6D), suggesting that CRTC/CREB signal was responsible for regulating MetaLnc9 expression in NSCLC cells, with NONO involved.

Next, we analyzed the 2.5-kb MetaLnc9 promoter and found three potential CREB1 binding sites (Fig. 6E; JASPAR database: http://jaspar.genereg.net/; consensus sequence: 5′-TGACGTCA-3′). Furthermore, luciferase reporters containing promoter fragments lacking −1,130∼−178 nt region did not respond to CREB1 (Fig. 6F), suggesting the presence of a crucial CREB1-binding site in this region. These data, combined with the CREB1 motif prediction (Fig. 6E), suggest that the −245∼−252 nt element might contain the CREB1-binding site. Mutating this −245∼−252 nt element blocked the ability of CREB 1 to enhance the luciferase activity of the 2.5-kb MetaLnc9 promoter (Fig. 6G). Subsequent ChIP assays verified that CREB1 directly interacts with a binding site in the −245∼−252 nt region (Fig. 6H and I). Taken together, our data show that NONO regulates MetaLnc9 transcription through CRTC/CREB transcription.

Because MetaLnc9 physically interacted with NONO, we hypothesized that MetaLnc9 regulates its own expression through a feedback loop involving CRTC/CREB transcription. As expected, MetaLnc9 overexpression promoted the 2.5-kb promoter activity of itself in SPC-A-1 cells (Fig. 6J). Furthermore, the increased luciferase activity by MetaLnc9 overexpression could also be suppressed by NONO knockdown in these cells (Fig. 6K) but be stimulated by CREB1 overexpression (Fig. 6L). These data suggested that MetaLnc9 had a positive feedback regulation on itself via NONO/CREB1 complexes-mediated transcription. Moreover, enhanced MetaLnc9 expression promoted the interactions between NONO and CRTC2 (Fig. 6M), and the interaction between MetaLnc9 and CTRC2 was confirmed in SPC-A-1sci cells (Fig. 6N). These data support a model whereby MetaLnc9 acts as a coactivator with CRTC/CREB in a positive feedback loop that maintains a high steady-state level of itself.

Discussion

Similar to protein-coding genes, lncRNAs contribute dramatically to many biological processes (23). Recent studies have revealed that lncRNAs are involved in tumor metastasis progression (24, 25) and are clinically useful in diagnosis and prognosis (26). Lung cancer is the leading cause of cancer-related death; thus, improved predictive biomarkers are necessary to ensure that cancer patients are provided with the most effective treatments. To identify a lncRNA signature for NSCLC metastasis, we performed lncRNA expression profiling on cell lines with different metastatic abilities and the same genomic background, which were derived from SPC-A-1 cells using a mouse-screening model (19). Our expression and functional data show that MetaLnc9 is an oncogenic lncRNA in NSCLC cells. Moreover, we provide mechanistic insights into MetaLnc9 as an AKT/mTOR pathway activator and a critical regulator of CRTC/CREB target genes via interactions with protein partners.

MetaLnc9 is significantly upregulated in highly metastatic SPC-A-1sci cells, which were derived from SPC-A-1 cells via 3-rounds of *in vivo* selection in NOD/SCID mice (19). Importantly, high levels of MetaLnc9 in lung cancer tissues are correlated with poor tumor TNM stage and tumor metastasis. Our results also strongly suggested that MetaLnc9 is related to the clinical severity of NSCLC patients, and can be considered as a clinical biomarker of prognosis in NSCLC. Consistently, we confirmed that MetaLnc9 enhanced the migration and invasion of lung cancer cells *in vitro* and *in vivo* and found that interactions of PGK1 and NONO with MetaLnc9 are responsible for the oncogenic function of this lncRNA. PGK1, a key component of the glycolytic pathway, is a rate-limiting enzyme that catalyzes the conversion of 1,3-bisphospholgycerate (1,3-BPG) and ADP into 3-phosphoglycerate (3-PG) and ATP. This PGK-catalyzed reaction is the first ATP-yielding step of glycolysis and is essential for energy production via the glycolytic pathway of aerobes and the fermentation of anaerobes in most living cells (27, 28). Extracellular PGK1 secreted by tumors acts as a disulfide reductase that can cleave plasminogen, generating the vascular inhibitor angiostatin in gastric cancer (29, 30). Our results also confirm that PGK1 siRNAs inhibit lung cancer cell migration and invasion and that PGK1 physically interacts with the functional fragment of MetaLnc9. We provide evidence that MetaLnc9 activates the Akt/mTOR pathway in NSCLC cells, consistent with Akt activation by MetaLnc9 in prostate cancer cells (31). PGK1 likely promotes tumor cell invasion by activating the AKT and ERK pathways in prostate tumor cells (32). It has been well-known that PGK1 plays key role on glycolytic ATP production (27). There have been several lines of evidences suggesting that mitochondrial ATP production can activate the PI3K-AKT pathway through P2 receptors in several cell types (33, 34). Moreover, an increased cytosolic free calcium level, the crucial second messenger of the ATP/P2 receptor-signaling pathway, can activate PI3K by direct association with its p85 regulatory subunit, leading to activation of the AKT/mTOR pathway (35). Consistently, PGK1 activates the AKT and ERK pathways in prostate cancer cells, resulting in the promotion of cell invasion (30). Our results suggest that MetaLnc9 posttranslationally regulates PGK1 by blocking its ubiquitin-mediated degradation. It is not surprising to find that MetaLnc9 could activate the Akt/mTOR pathway in NSCLC cells, thus promoting the metastasis of these cells.

Another protein partner of MetaLnc9 detected in NSCLC cells is P54nrb/NonO (NONO). Unlike PGK1, NONO is a nuclear RNA-binding protein that is involved in many cellular events, such as pre-mRNA processing, transcription, and the nuclear retention of hyperedited RNAs (36, 37). NONO directly binds the 5′ splice site in pre-mRNAs, as well as the CTD domain of RNA polymerase and snRNP U5 (38). Recent studies have demonstrated that NONO is a major component of nuclear paraspeckles and interacts with the noncoding RNA NEAT1/Vinc1 (39, 40). Our study found that MetaLnc9 interacts with both PGK1 and NONO but that the two proteins did not bind each other. Given the regulatory effect of MetaLnc9 on PGK1 and the distribution of MetaLnc9 (both cytoplasmic and nuclear), PGK1 (cytoplasmic) and NONO (nuclear), we speculate that PGK1 is a functional downstream

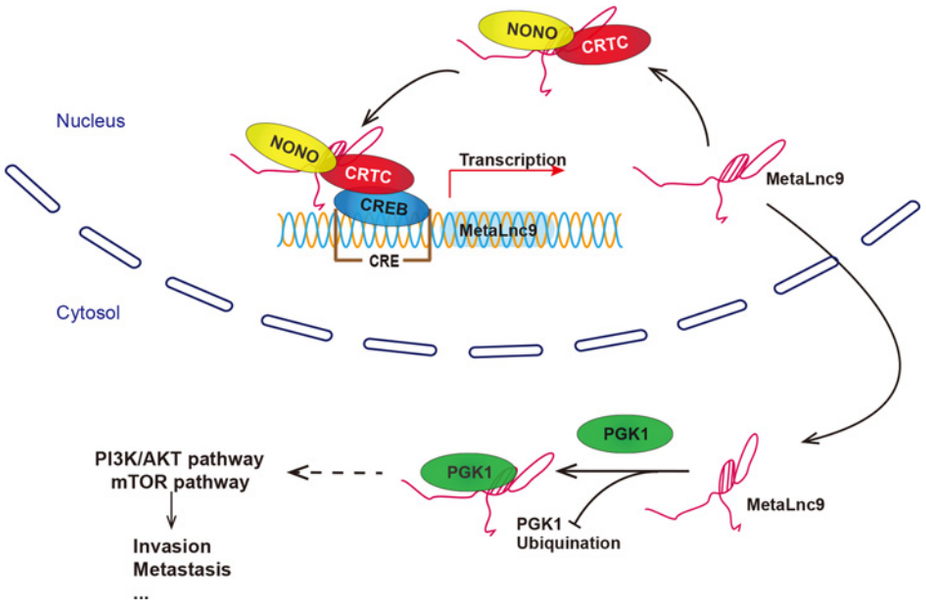

Figure 7.
Integrated model depicting lncRNA MetaLnc9 as an activator in NSCLC cell metastasis. The working model shows that MetaLnc9 exerts its oncogenic activity by interacting with and stabilizing PGK1, thereby activating PI3K/Akt/mTOR signaling in NSCLC cells. Moreover, MetaLnc9 interacts with NONO and participates in CREB/CRTC-mediated transcription, creating a positive feedback loop.

target of MetaLnc9 in the cytosol, whereas NONO may function as an upstream regulator of this lincRNA in the nucleus. Our data strongly support a critical role for NONO in the transcriptional regulation of MetaLnc9 via CRTC/CREB1 (22). Interestingly, MetaLnc9 regulates its own expression through a positive feedback loop by promoting the recruitment of NONO and CRTC2. Moreover, it should be noted that MetaLnc9 over-expression may have led to the enrichment of cAMP signaling pathway in our RNA-seq profiling, indicating that MetaLnc9 likely participates in transcriptional regulation in the NONO/CRTC/CREB complex. Several CRTC/CREB1 target genes, such as NEDD9, have been implicated in regulating EMT and the metastasis of NSCLC cells (41, 42). Another report demonstrated that LINC00473 is also essential for maintaining LKB1-inactivated lung cancer cell growth and survival by interacting with NONO and mediating CRTC/CREB1 transcription (17). However, in our screening, LINC00473 was significantly downregulated in SPC-A-1-sci cells compared with SPC-A-1 cells, and low levels of LINC00473 correlated with NSCLC metastasis. Moreover, LKB1 mutation status was not obviously associated with the expression of MetaLnc9 (17). These results offer clues into the role of MetaLnc9 in LKB1-independent NSCLC cells and should be investigated further.

In summary, we identified a metastasis-related lncRNA MetaLnc9 that is associated with poor patient survival and that may be useful for classifying metastasis status in human NSCLC. MetaLnc9 enhances NSCLC cell metastasis *in vitro* and *in vivo*, supporting the notion that targeting this lincRNA is an effective therapeutic strategy for NSCLC metastasis. MetaLnc9 interacts with PGK1 and activates AKT/mTOR signaling in NSCLC cells. Finally, we identified a function for MetaLnc9 in the transcriptional regulation of CRTC/CREB1 target genes by interacting with NONO (Fig. 7). Collectively, our study offers mechanistic insights into the oncogenic roles of MetaLnc9 and the pivotal effects of MetaLnc9 as a biomarker and therapeutic target for NSCLC metastasis.

Disclosure of Potential Conflicts of Interest

No potential conflicts of interest were disclosed.

Authors' Contributions

Conception and design: T. Yu, Y. Zhao, J. Li, B. Chen, H. Lin, L. Liu, M. Yan, X. He, M. Yao
Development of methodology: T. Yu, Z. Hu, J. Li, D. Chu, J. Zhang, B. Chen, X. Zhang, H. Lin, L. Liu
Acquisition of data (provided animals, acquired and managed patients, provided facilities, etc.): T. Yu, D. Chu, J. Zhang, Z. Li, B. Chen, H. Lin, M. Yan
Analysis and interpretation of data (e.g., statistical analysis, biostatistics, computational analysis): T. Yu, Y. Zhao, J. Li, D. Chu, Z. Li, B. Chen, X. Zhang, S. Li, H. Lin, M. Yao
Writing, review, and/or revision of the manuscript: T. Yu, Y. Zhao, B. Chen, H. Pan, H. Lin, X. He, M. Yao
Administrative, technical, or material support (i.e., reporting or organizing data, constructing databases): D. Chu, Z. Li, H. Pan, M. Yan
Study supervision: Y. Zhao, L. Liu, X. He, M. Yao

Acknowledgments

We are grateful for Dr. Didier Trono for sharing pWPXL lentivirus plasmids.

Grant Support

This work was supported in part by grants from National Natural Science Foundation of China (no. 81472176 to M. Yao; no. 81502488 to M. Yan), the National Key Program for Basic Research of China (973; no. 2015CB553905 to W. Qin) and the Natural Science Foundation of Shanghai (no. 15ZR1439000 to H. Lin).

The costs of publication of this article were defrayed in part by the payment of page charges. This article must therefore be hereby marked *advertisement* in accordance with 18 U.S.C. Section 1734 solely to indicate this fact.

Received March 10, 2017; revised July 27, 2017; accepted September 5, 2017; published OnlineFirst September 18, 2017.

References

1. Siegel R, Ma J, Zou Z, Jemal A. Cancer statistics, 2014. CA Cancer J Clin 2014;64:9–29.
2. Reck M, Popat S, Reinmuth N, De Ruysscher D, Kerr KM, Peters S. Metastatic non-small-cell lung cancer (NSCLC): ESMO Clinical Practice Guidelines for diagnosis, treatment and follow-up. Ann Oncol 2014;25:iii27–39.
3. Field JK, Oudkerk M, Pedersen JH, Duffy SW. Prospects for population screening and diagnosis of lung cancer. Lancet 2013;382:732–41.
4. Chen W, Zheng R, Baade PD, Zhang S, Zeng H, Bray F, et al. Cancer statistics in China, 2015. CA Cancer J Clin 2016;66:115–32.
5. Dela Cruz CS, Tanoue LT, Matthay RA. Lung cancer: epidemiology, etiology, and prevention. Clin Chest Med 2011;32:605–44.
6. Mercer TR, Dinger ME, Mattick JS. Long non-coding RNAs: insights into functions. Nat Rev Genet 2009;10:155–9.
7. Hacisuleyman E, Goff LA, Trapnell C, Williams A, Henao-Mejia J, Sun L, et al. Topological organization of multichromosomal regions by the long intergenic noncoding RNA Firre. Nat Struct Mol Biol 2014;21:198–206.
8. Batista PJ, Chang HY. Long noncoding RNAs: cellular address codes in development and disease. Cell 2013;152:1298–307.
9. Gupta RA, Shah N, Wang KC, Kim J, Horlings HM, Wong DJ, et al. Long non-coding RNA HOTAIR reprograms chromatin state to promote cancer metastasis. Nature 2010;464:1071–6.
10. Hall JR, Messenger ZJ, Tam HW, Phillips SL, Recio L, Smart RC. Long noncoding RNA lincRNA-p21 is the major mediator of UVB-induced and p53-dependent apoptosis in keratinocytes. Cell Death Dis 2015;6:e1700.
11. Huarte M, Guttman M, Feldser D, Garber M, Koziol MJ, Kenzelmann-Broz D, et al. A large intergenic noncoding RNA induced by p53 mediates global gene repression in the p53 response. Cell 2010;142:409–19.
12. Prensner JR, Iyer MK, Balbin OA, Dhanasekaran SM, Cao Q, Brenner JC, et al. Transcriptome sequencing across a prostate cancer cohort identifies PCAT-1, an unannotated lincRNA implicated in disease progression. Nat Biotechnol 2011;29:742–9.
13. Wang P, Xue Y, Han Y, Lin L, Wu C, Xu S, et al. The STAT3-binding long noncoding RNA lnc-DC controls human dendritic cell differentiation. Science 2014;344:310–3.
14. Li Y, Wang Z, Shi H, Li H, Li L, Fang R, et al. HBXIP and LSD1 Scaffolded by lncRNA hotair mediate transcriptional activation by c-Myc. Cancer Res 2016;76:293–304.
15. Ling H, Spizzo R, Atlasi Y, Nicoloso M, Shimizu M, Redis RS, et al. CCAT2, a novel noncoding RNA mapping to 8q24, underlies metastatic progression and chromosomal instability in colon cancer. Genome Res 2013;23:1446–61.
16. Yang F, Zhang H, Mei Y, Wu M. Reciprocal regulation of HIF-1alpha and lincRNA-p21 modulates the Warburg effect. Mol Cell 2014;53:88–100.
17. Chen Z, Li JL, Lin S, Cao C, Gimbrone NT, Yang R, et al. cAMP/CREB-regulated LINC00473 marks LKB1-inactivated lung cancer and mediates tumor growth. J Clin Invest 2016;126:2267–79.
18. Lan X, Yan J, Ren J, Zhong B, Li J, Li Y, et al. A novel long noncoding RNA Lnc-HC binds hnRNPA2B1 to regulate expressions of Cyp7a1 and Abca1 in hepatocytic cholesterol metabolism. Hepatology 2016;64:58–72.
19. Jia D, Yan M, Wang X, Hao X, Liang L, Liu L, et al. Development of a highly metastatic model that reveals a crucial role of fibronectin in lung cancer cell migration and invasion. BMC Cancer 2010;10:364.
20. Pruitt KD, Tatusova T, Maglott DR. NCBI reference sequences (RefSeq): a curated non-redundant sequence database of genomes, transcripts and proteins. Nucleic Acids Res 2007;35:D61–5.
21. Suzuki A, Makinoshima H, Wakaguri H, Esumi H, Sugano S, Kohno T, et al. Aberrant transcriptional regulations in cancers: genome, transcriptome and epigenome analysis of lung adenocarcinoma cell lines. Nucleic Acids Res 2014;42:13557–72.
22. Amelio AL, Miraglia LJ, Conkright JJ, Mercer BA, Batalov S, Cavett V, et al. A coactivator trap identifies NONO (p54nrb) as a component of the cAMP-signaling pathway. Proc Nat Acad Sci U S A 2007;104:20314–9.
23. Hombach S, Kretz M. Non-coding RNAs: Classification, Biology and Functioning. Adv Exp Med Biol 2016;937:3–17.
24. Jiang C, Li X, Zhao H, Liu H. Long non-coding RNAs: potential new biomarkers for predicting tumor invasion and metastasis. Mol Cancer 2016;15:62.
25. Schmitt AM, Chang HY. Long Noncoding RNAs in Cancer Pathways. Cancer Cell 2016;29:452–63.
26. Cabanski CR, White NM, Dang HX, Silva-Fisher JM, Rauck CE, Cicka D, et al. Pan-cancer transcriptome analysis reveals long noncoding RNAs with conserved function. RNA Biol 2015;12:628–42.
27. Scopes RK.Studies with a reconstituted muscle glycolytic system. The rate and extent of creatine phosphorylation by anaerobic glycolysis. Biochem J 1973;134:197–208.
28. Wang S, Jiang B, Zhang T, Liu L, Wang Y, Wang Y, et al. Insulin and mTOR Pathway Regulate HDAC3-Mediated Deacetylation and Activation of PGK1. PLoS Biol 2015;13:e1002243.
29. Zieker D, Konigsrainer I, Traub F, Nieselt K, Knapp B, Schillinger C, et al. PGK1 a potential marker for peritoneal dissemination in gastric cancer. Cell Physiol Biochem 2008;21:429–36.
30. Lay AJ, Jiang XM, Kisker O, Flynn E, Underwood A, Condron R, et al. Phosphoglycerate kinase acts in tumour angiogenesis as a disulphide reductase. Nature 2000;408:869–73.
31. Wang L, Han S, Jin G, Zhou X, Li M, Ying X, et al. Linc00963: a novel, long non-coding RNA involved in the transition of prostate cancer from androgen-dependence to androgen-independence. Int J Oncol 2014;44:2041–9.
32. Wang J, Ying G, Wang J, Jung Y, Lu J, Zhu J, et al. Characterization of phosphoglycerate kinase-1 expression of stromal cells derived from tumor microenvironment in prostate cancer progression. Cancer Res 2010;70:471–80.
33. Osorio-Fuentealba C, Contreras-Ferrat AE, Altamirano F, Espinosa A, Li Q, Niu W, et al. Electrical stimuli release ATP to increase GLUT4 translocation and glucose uptake via PI3Kgamma-Akt-AS160 in skeletal muscle cells. Diabetes 2013;62:1519–26.
34. Ishikawa M, Iwamoto T, Nakamura T, Doyle A, Fukumoto S, Yamada Y. Pannexin 3 functions as an ER Ca(2+) channel, hemichannel, and gap junction to promote osteoblast differentiation. J Cell Biol 2011;193:1257–74.
35. Cheng A, Wang S, Yang D, Xiao R, Mattson MP. Calmodulin mediates brain-derived neurotrophic factor cell survival signaling upstream of Akt kinase in embryonic neocortical neurons. J Biol Chem 2003;278:7591–9.
36. Basu A, Dong B, Krainer AR, Howe CC. The intracisternal A-particle proximal enhancer-binding protein activates transcription and is identical to the RNA- and DNA-binding protein p54nrb/NonO. Mol Cell Biol 1997;17:677–86.
37. Kameoka S, Duque P, Konarska MM. p54(nrb) associates with the 5′ splice site within large transcription/splicing complexes. EMBO J 2004;23:1782–91.
38. Emili A, Shales M, McCracken S, Xie W, Tucker PW, Kobayashi R, et al. Splicing and transcription-associated proteins PSF and p54nrb/nonO bind to the RNA polymerase II CTD. Rna 2002;8:1102–11.
39. Clemson CM, Hutchinson JN, Sara SA, Ensminger AW, Fox AH, Chess A, et al. An architectural role for a nuclear noncoding RNA: NEAT1 RNA is essential for the structure of paraspeckles. Mol Cell 2009;33:717–26.
40. Hutchinson JN, Ensminger AW, Clemson CM, Lynch CR, Lawrence JB, Chess A. A screen for nuclear transcripts identifies two linked noncoding RNAs associated with SC35 splicing domains. BMC Genom 2007;8:39.
41. Kondo S, Iwata S, Yamada T, Inoue Y, Ichihara H, Kichikawa Y, et al. Impact of the integrin signaling adaptor protein NEDD9 on prognosis and metastatic behavior of human lung cancer. Clin Cancer Res 2012;18:6326–38.
42. Miao Y, Li AL, Wang L, Fan CF, Zhang XP, Xu HT, et al. Overexpression of NEDD9 is associated with altered expression of E-Cadherin, beta-Catenin and N-Cadherin and predictive of poor prognosis in non–small cell lung cancer. Pathol Oncol Res 2013;19:281–6.